

A Study of Soft and Hard Breakdown—Part II: Principles of Area, Thickness, and Voltage Scaling

Muhammad Ashraful Alam, *Senior Member, IEEE*, Bonnie E. Weir, *Member, IEEE*, and Paul J. Silverman

Abstract—Based on the theory of soft and hard breakdown established in Part I of this paper [10], we now study the principles of area, thickness, voltage, and circuit configuration dependence of hard and soft breakdown. These scaling principles allow us to conclude that breakdown in ultrathin oxides stressed at operating voltages (1.0–1.5 V) can never be hard, which should allow a more relaxed reliability specification for these oxides.

Index Terms—Hard breakdown, MOS devices, reliability, semiconductor device modeling, soft breakdown.

I. INTRODUCTION

IN this paper, we begin analyzing the available experimental data [1]–[7], (based on the theoretical framework developed in Part I of this paper [10], to understand the principles of area scaling (Section II), voltage scaling (Section III), and thickness scaling (Section IV) for the soft breakdown phenomenon [7]. We also show, in Section V, that it is the power dissipation, not the stored energy, which determines the severity of oxide breakdown [7], [8], [9]. This discussion provides a framework to explain the available experiments consistently, and allows us, in Section V, to scale these results to thinner oxides with smaller areas operating at lower voltages. Theoretically, our analysis will be based on verifying the predictions of (3)–(5)¹, given the statistical properties of the percolation conductance (G_p) discussed in [10], and given the fact that the various terms of (3)–(5) depend on area, thickness, and stress conditions in different ways. Rather than solving for the entire probability distribution function (pdf) of G_p , we can solve (3)–(8) for the maximum and minimum values of the voltage across the capacitor ($V^{(\min)}(t)$, $V^{(\max)}(t)$) and power dissipation through the percolation path ($P^{(\min)}(t)$, $P^{(\max)}(t)$), by using the maximum and minimum values of the percolation conductance ($G_o^{(\max)}$, $G_o^{(\min)}$). In this way, we can delineate the boundaries of the pdf of the voltage and power transient just by solving two equations, which will be sufficient to indicate the trends of the experimental observations. Based on the detailed analysis of the percolation conductance in [10], we assume that although G_o is area independent, it does depend weakly on thickness [10, Fig. 5], and that the ratio $G_o^{(\max)}/G_o^{(\min)}$ is 4 to 6. For simplicity, we ignore the time-dependent conductance evolution during the breakdown transient, i.e., we assume $G_p(t) = G_p(t = 0)$. Although this assumption will introduce

larger error-bars in our results, the trends predicted, over a wide range of parameters, will still be accurate [7].

II. AREA SCALING

The capacitors used to determine the physical properties of oxide films often have large areas. However, the areas of transistors in IC are usually orders of magnitude smaller. The basic question, then, is: How do the properties of soft and hard breakdown (i.e., magnitude of the postbreakdown currents or voltages, dependence on stress conditions, etc.) translate as a function of different oxide areas? Consider the experimental data shown in Fig. 2. Each short horizontal dash in this plot represents a specific sample with a certain area (x -axis) and a certain postbreakdown voltage (y -axis). The distribution of these postbreakdown voltages for different samples with the same capacitor area results from the statistical distribution of percolation conductivities. Given that all the capacitors were stressed at constant current density (same stress voltage), Fig. 2 shows two contradictory trends:

- soft breakdown gets softer with increasing area; in other words, the difference between pre- and postbreakdown voltages for soft breakdown decreases with area;
- yet, hard breakdown becomes more probable for capacitors with larger areas. (e.g., the gray dashed line in Fig. 2).

To understand these trends for constant current stress, consider the prebreakdown current–voltage (I – V) characteristics (see Fig. 1) of capacitors with two different areas: A_{large} (solid line) and A_{small} (dashed line). For a given prebreakdown stress voltage $J(V, A_{\text{large}}) = J(V, A_{\text{small}})$ and therefore, $I_B = (A_{\text{large}}/A_{\text{small}})I_A$ corresponding to points A and B in Fig. 1. After breakdown, V_{postBD} are given by points C and D on the area-independent, almost-coincident, postbreakdown $I_{\text{perc}} - V$ curves. This explains, qualitatively, why the final soft breakdown voltages for larger capacitors are larger and why the breakdowns *appear* softer for larger capacitors (see Fig. 2). However, the power dissipation for the larger capacitors ($I_B \Delta V_{\text{BD}}$) is much larger than that of smaller capacitors ($I_A \Delta V_{\text{AC}}$), (because, although $\Delta V_{\text{AC}} > \Delta V_{\text{BD}}$, $I_B \gg I_A$) which makes hard breakdown more probable for larger area capacitors, again confirming the observations of Fig. 2. Having qualitatively explained the trends, we can now validate these conclusions quantitatively by solving (3)–(6) numerically. For each stress current, the maximum and minimum values of G_0 [in (3)] determine $V_{\text{postBD}}^{(\min)}$ (dashed line with open squares, Fig. 2) and $V_{\text{postBD}}^{(\max)}$ (dotted line with open circles, Fig. 2), respectively. The simulation results show good agreement with experimental data for post-soft-breakdown voltages, and Fig. 3

Manuscript received March 20, 2001; revised September 17, 2001. The review of this paper was arranged by Editor G. Groeseneken.

The authors are with Agere Systems, Murray Hill, NJ 07974 (e-mail: alam@agere.com).

Publisher Item Identifier S 0018-9383(02)00821-3.

¹All equation numbers refer to [10].

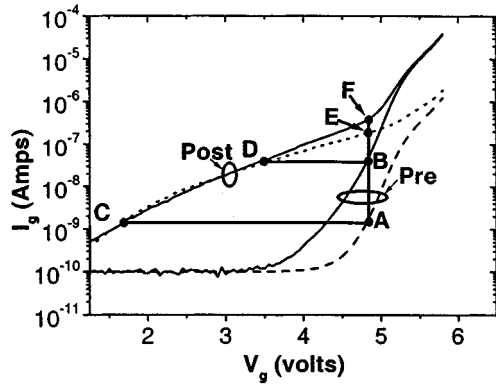


Fig. 1. I - V characteristics (for two different areas) before and after soft breakdown. Note that the postbreakdown current is uncorrelated to area of the capacitor. Before breakdown, both the capacitors are stressed at the same voltage so that the larger area capacitor (point B) has more total current than the smaller area capacitor (point A). The trajectory of I - V transient during breakdown for constant current stress (horizontal lines, end points C and D), and constant voltage stress (vertical lines, end points E and F) determine the final breakdown characteristics of these oxides.

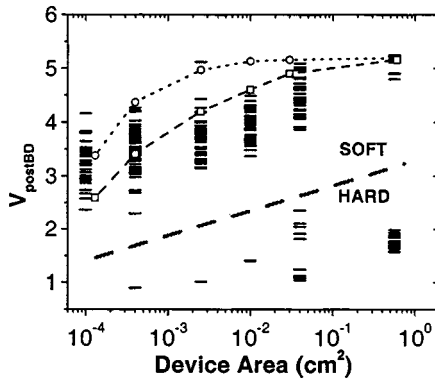


Fig. 2. Area dependence of oxide breakdown for constant current stress. Equivalent circuit simulation, with $G_o^{(\max)}$ (dotted line, open circles) and $G_o^{(\min)}$ (dashed line, open squares), reproduces the correct range of experimentally observed postbreakdown voltages. Note that as the area of the capacitor gets larger, the postbreakdown voltages also become large (compare point D to point C, Fig. 1).

shows how $\{P_{\text{perc}}\}$ [(see (7))] increases with capacitor area making hard breakdown more probable for larger capacitors. According to the discussion in Section II, if the range of P_{perc} (based on $G_o^{(\min)}$ and $G_o^{(\max)}$) is completely above or completely below P_{crit} (Fig. 3, horizontal dashed lines without symbols) only hard or only soft breakdown is possible. Otherwise, P_{perc} will exceed P_{crit} for some of the samples leading to hard breakdown, for others P_{perc} will stay below P_{crit} leading to soft breakdown, and therefore, the breakdown distribution will be bimodal. These observations, based on Fig. 3, are confirmed in Fig. 2.

Next, consider the consequences of area difference for constant voltage stress. Fig. 4 shows two distinct trends:

- for soft breakdown, the postbreakdown current, I_{postBD} , is essentially area independent;
- the fraction of oxides having soft breakdown does not depend on the capacitor area.

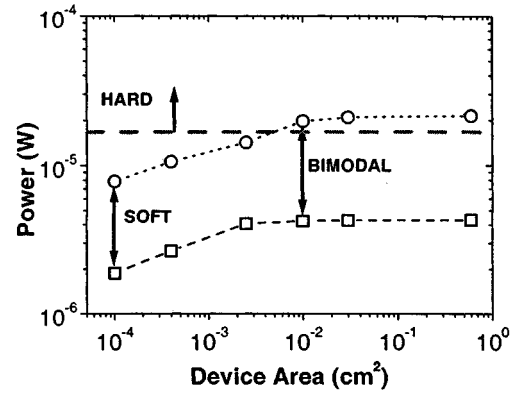


Fig. 3. Power dissipation through the percolation path increases with area for constant current stress, explaining why hard breakdown becomes more probable (see Fig. 2) with larger capacitor area. For very small capacitors, $P_{\text{perc}} < P_{\text{crit}}$, so all the breakdowns are soft. However, for larger area capacitors, P_{perc} can exceed P_{crit} for some of the capacitors resulting in hard breakdown and explaining the bimodal breakdown distribution in Fig. 2.

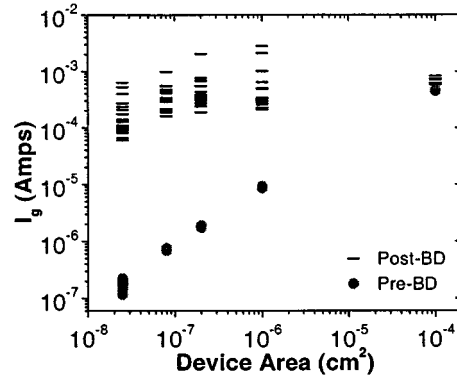


Fig. 4. For constant voltage stress, the prebreakdown current (filled circles) scales linearly with area (see Fig. 1). After breakdown, both the postbreakdown currents (short dashes) as well as the fraction of oxides undergoing soft breakdown, are surprisingly insensitive to the area of the capacitor. In this particular case, all of the breakdown events (short dashes) are soft (as determined from the δ values of their postbreakdown I - V characteristics).

Both of these trends are in sharp contrast to those observed for constant current stress. To understand this, we refer to the I - V characteristics (Fig. 1), which shows that while the prebreakdown currents scales linearly with area for a given stress voltage (points A and B), they translate vertically to nearly coincident postbreakdown currents (points E and F). This explains why the postbreakdown currents in Fig. 4 are nearly area-independent. The distribution of the postbreakdown current simply reflects the distribution of the percolation conductance. Moreover, since the stress voltage is held constant, the capacitor can not discharge during the breakdown transient, so the contribution of its displacement current vanishes [comments following (6) and (8)]. Therefore, the net power dissipation $P_{\text{perc}} \sim E^2 G_p$ is independent of the area of the capacitor, and depends solely on the stress voltage. More specifically, Fig. 1 shows that $P_{AE} = V_A(I_E - I_A) \sim V I_E$ will be almost exactly equal to $P_{BF} = V_B(I_F - I_A) \sim V I_F$, because $I_E \sim I_F$, and because I_A, I_B are negligible in comparison. Once again, if $P_{\text{perc}} < P_{\text{crit}}$, soft breakdown will occur, otherwise hard breakdown will follow.

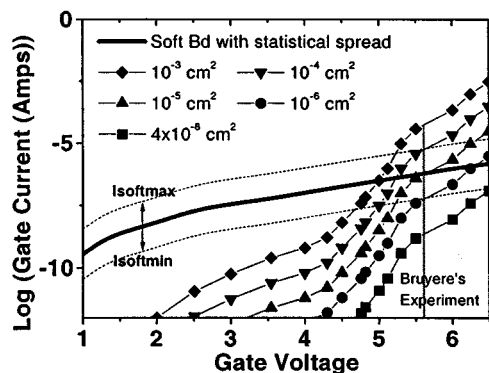


Fig. 5. Current after soft breakdown versus direct tunneling current for different areas. Soft breakdown ($I_{\text{perc}}^{\text{avg}}$)—solid line, and ΔI_{perc} —dotted lines) becomes more difficult to detect for large area capacitors particularly if the stress voltage is large, say, $V = 5.6$ V, here).

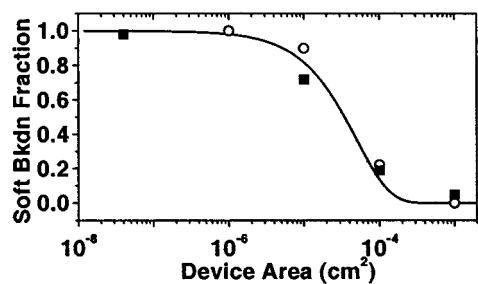


Fig. 6. Experimental data (solid squares) and interpretation (continuous solid line) from [6] for soft breakdown fraction obtained compared to our calculation (open symbols) assuming a 10% change in current was used to detect breakdown occurrence.

But in either case, as seen in Fig. 4, area plays no role in determining the breakdown characteristics.

Note that it is very important to determine the first breakdown, be it soft or hard, for any rigorous analysis of the breakdown dynamics. For large area capacitors, this determination may be particularly difficult. For example, Fig. 5 (a replot of Fig. 1) shows that if the area of the capacitor is too large (e.g., $A = 10^{-3}$ cm², diamond symbol, Fig. 5) for a given stress voltage, it is possible that the first breakdown can be completely missed due to the large background tunneling current, i.e., $AJ_{\text{stress}} \gg I_{\text{perc,soft}}$, so that the total current $I_T = AJ_{\text{stress}} + I_{\text{perc}} \sim AJ_{\text{stress}}$. In this case, no change in current is detected, and one may believe, incorrectly, that no breakdown has occurred. The only time breakdown is detected for large area capacitors is when hard breakdown short-circuits the capacitor so that $AJ_{\text{stress}} < I_{\text{perc,hard}}$ and $I_T = AJ_{\text{stress}} + I_{\text{perc,hard}} \sim I_{\text{perc,hard}}$ so that the change in the total current becomes noticeable. Indeed, this may lead one to believe, incorrectly, that there is higher probability of hard breakdown for a larger area capacitor even for constant voltage stress. In fact, this possible misinterpretation has even been presented as evidence for new breakdown models which claim that soft and hard breakdown are caused by different types of traps [6]. To compute the probability of the missed soft breakdown events for a large area capacitor, assume that detecting a breakdown requires at least a 100% change in the total current, (i.e., $dI/I = \xi$), therefore the detection of soft

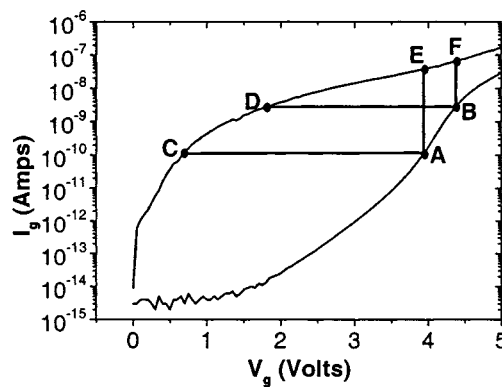


Fig. 7. I – V characteristics for an oxide stressed with different currents before (e.g., points A and B) and after breakdown (e.g., points C and D for constant current stress and points E and F for constant voltage stress). The power dissipation during the breakdown transient determines the fraction of hard and soft breakdown events.

breakdown requires [$dI = \xi AJ_{\text{stress}}, I + dI < I_{\text{perc,softmin}}$]. Using the data from [6] for J_{stress} and I_{perc} , we see that, as anticipated, the fraction of the missed breakdown exactly follows the profile of fraction of “hard breakdown” (see Fig. 5 and 6). Therefore, the increased incidence of hard breakdown in [6] simply reflects the difficulty in detecting soft breakdown events, and does not contradict our assertion that for constant voltage stress, the probability of soft breakdown is independent of area.

III. STRESS VOLTAGE (CURRENT) SCALING

The analysis of the last section allows us to translate breakdown results from large area capacitors to small area transistors (for a given stress current), and to design better test structures with appropriate areas so that hard and soft breakdown can easily be detected. In this section, we consider the effect of changing the stress currents and stress voltages on soft and hard breakdown. This analysis will help translate the test results obtained from higher stress voltages (or currents) to actual operating conditions.

Considering the pre- and postbreakdown I – V characteristics shown in Fig. 7. If, before breakdown, two capacitors (the same oxide thickness and same area) are stressed at two different currents, I_A and I_B , such that $I_B > I_A$, then obviously $V_B > V_A$. Under constant current stress, the final voltages after breakdown for these capacitors will be V_C and V_D , such that $V_C < V_D$. Therefore, we expect that larger prebreakdown stress current should produce larger postbreakdown voltage. Moreover, since $(dV/dI)|_{\text{perc}} > (dV/dI)|_{\text{tunnel}}$, the difference between pre- and postbreakdown voltages are such that $(V_B - V_D) < (V_A - V_C)$. In other words, the difference in the pre- and postbreakdown voltages becomes smaller with larger stress current. Both these predicted trends are validated in Fig. 8. The solution of (3)–(9) for these specific stress conditions correctly anticipates the range of final breakdown voltages corresponding to the statistical distribution of percolation conductance (dotted and dashed lines). Similarly, for constant current stress, the power dissipation $P_{AC} = I_A(V_A - V_C)$ is much smaller than $P_{BD} = I_B(V_B - V_D)$ (see Fig. 7). This is because, although $(V_A -$

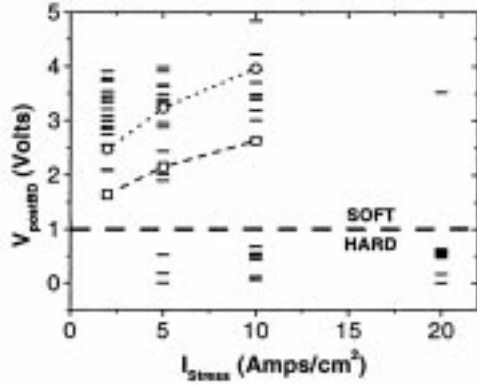


Fig. 8. The breakdown distribution, as a function of stress current, is plotted (short horizontal dashes: experimental data; dotted and dashed line: simulation). The postbreakdown voltage increases with stress current and so does the probability of harder breakdown. The predictions of the postbreakdown voltages from (3)–(9), agree with the experimental data reasonably well.

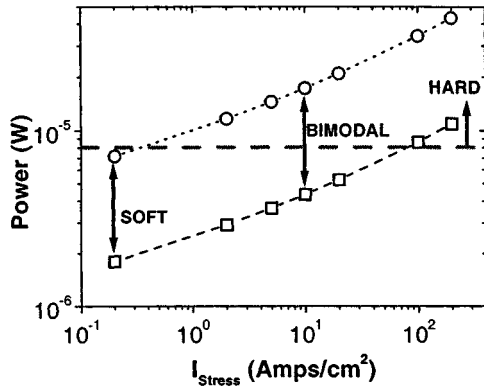


Fig. 9. Power dissipation through the oxide (dotted line, open circle for G_o^{\max} , dashed line, open squares, for G_o^{\min}) at low stress current is much smaller than the critical power density resulting mostly in soft breakdown. For high stress current, power dissipation always exceeds critical power density ensuring hard breakdown. In between, the breakdown is bimodal.

$V_C > (V_B - V_D)$, $I_B \gg I_A$. Therefore, we expect the number of hard breakdown events to increase with increasing stress current. These conclusions about soft and hard breakdown are supported by both detailed measurements and quantitative numerical results [based on the solution of (3)–(8)] in Figs. 8 and 9.

For constant voltage stress, based on the pre- and post-breakdown $I-V$ characteristics in Fig. 7, one expects the final postbreakdown current to increase slowly with increasing stress voltages (points E and F). Referring to Fig. 10, we find that this predicted slow increase in the I_{postBD} in the soft breakdown regime ($I_{\text{postBD}} < 30 \mu\text{A}$) is indeed observed experimentally. In addition, the power dissipation through the percolation path increases with increasing stress voltage, because $V_B > V_A$ and $I_F > I_E$ (see Fig. 7), and $P_{AE} \sim I_E V_A$ and $P_{BF} \sim I_F V_B$, so that $P_{BF} > P_{AE}$. Therefore, hard breakdown is more probable for larger stress voltages as seen in Fig. 10.

We explore the effect of constant voltage stress in some more detail in Fig. 11, which shows the percolation model predictions for $G_o - T_{\text{BD}}$ distribution [10, Fig. 7]. This distribution is oval shaped. For constant voltage stress, as the stress voltage

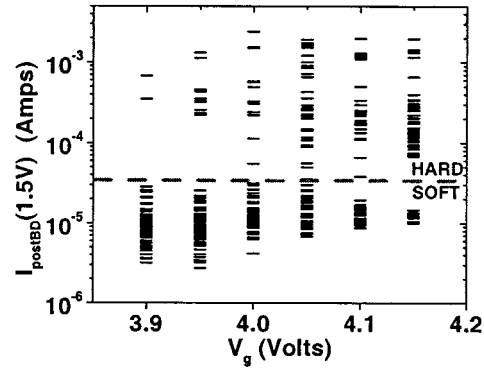


Fig. 10. For constant voltage stress, the postbreakdown current increases with increasing stress voltage. Moreover, a rise in the power dissipation with higher stress voltage, $P \sim V_{\text{stress}} I_{\text{perc}} |_{CVS}$, makes harder breakdown ($I_{\text{post}} > 30 \mu\text{A}$) more probable.

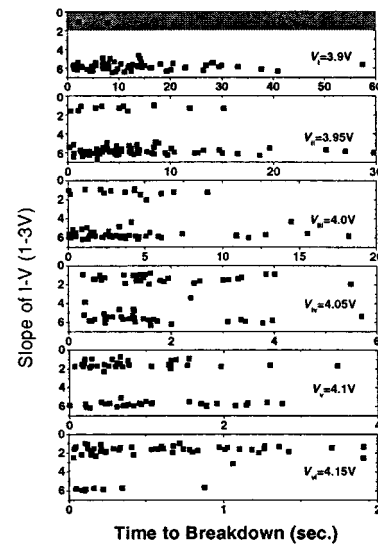
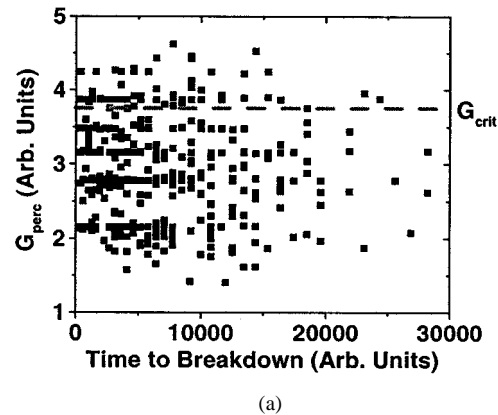


Fig. 11. (a) Theoretically predicted conductivity versus time-to-breakdown for an oxide thickness = $2 \times$ (trap-diameter). Each data point represents one sample. The horizontal line represents the critical conductivity, $G_{\text{crit}} \sim P_{\text{crit}}/V^2$, below which all breakdowns are hard, and above which all breakdowns are soft. This dividing line moves downwards with increasing voltage increasing the fraction of oxides that experiences hard breakdown. (b) Slope of $\ln(I_{\text{perc}}) - \ln(V)$ curve [δ , see (5)] obtained after breakdown. Note that $\delta < 2$ defines hard breakdown, and $\delta > 4$ defines soft breakdown. Each panel represents results for a given stress voltage corresponding to a given vertical position of the dividing line shown in (a). The oval-shape of (a) predicts the time versus slope relationships (indicating soft and hard breakdown) shown in the successive panels.

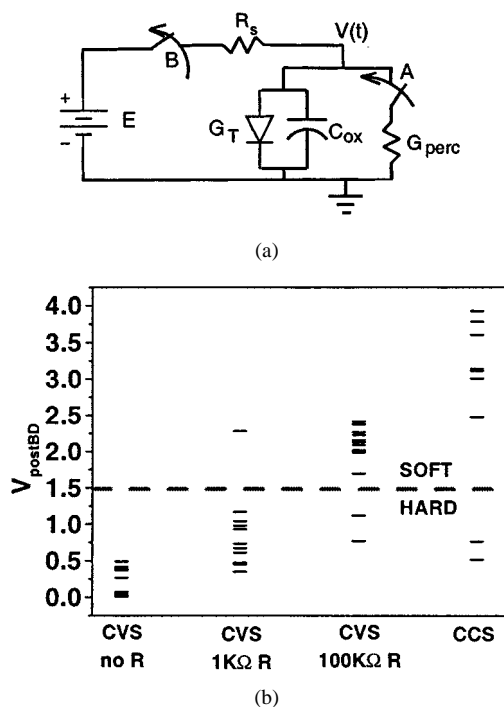


Fig. 12. (a) Adding a resistance R_s in series with the test capacitor modifies the power dissipation through the oxide, thereby controlling the fraction of hard and soft breakdown events. With $R_s = 0$, and $R_s = \infty$, these new circuits become identical to those in [10, Fig. 2(b)] with stress sources E and J_{stress} , respectively. (b) Constant voltage stress ($R_s = 0$) produces more hard breakdown (left) compared to constant current stress ($R_s = \infty$) (right) due to larger power dissipation through the percolation conductance at breakdown. The ratio of hard to soft breakdown changes smoothly as the R_s changes between the two extremes.

is increased, the conductance which separates the hard and soft breakdown, $G_{\text{crit}} \sim P_{\text{crit}}/V^2$, moves through the distribution like a knife (parallel to the x -axis) separating the samples into soft- and hard-broken populations. Our theory of soft and hard breakdown predicts that for such an oval-shaped $G_o - T_{\text{BD}}$ distribution, hard breakdown will occur at smaller T_{BD} for lower voltages, the two populations of hard and soft breakdown become symmetric with respect to the T_{BD} distribution at intermediate voltages, and finally, hard breakdown occurs at smaller T_{BD} for large voltages. The experimental data in Fig. 11(b) provides beautiful confirmation of these theoretical predictions. Note that Figs. 10 and 11(b) are based on the same set of experimental data.

Finally, it is important to understand that, for the same initial stress conditions, CCS results in somewhat softer breakdown, statistically speaking, compared to CVS [see Fig. 12(b)]. For CCS, the voltage across the sample decreases as a function of time during the breakdown transient, with a corresponding decrease in power dissipation through the percolation path (see [10, Fig. 2(c)]. Therefore, if the transistor can survive the first few microseconds of power dissipation, it is likely to survive without having a hard breakdown. On the other hand, CVS results in time-independent power dissipation through the percolation path ($P_{\text{perc}} \sim G_p E^2 / \delta$), so that after the initial transient up to the time τ_{ther} (see [10, Fig. 2(c)], the temperature of the percolation spot becomes constant. This sustained temperature rise makes it more probable that more samples will

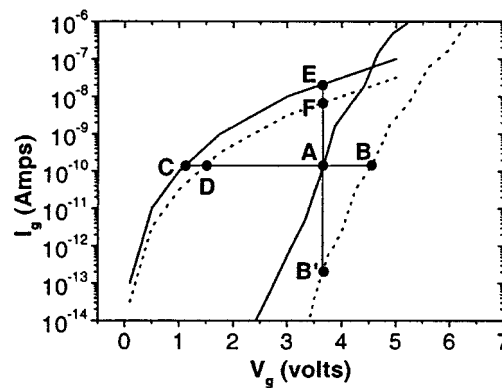


Fig. 13. $I-V$ characteristics for thin (4 nm, solid lines) and thick (5 nm, dashed line) oxides before (right pair, ABB') and after (left pair, CEDF) breakdown. Note that the dependence of postbreakdown current on oxide thickness is weaker than that of prebreakdown current. Points A and B on prebreakdown $I-V$ curve move to points C and D after breakdown with constant current stress. The final points for constant voltage stress are E and F.

have a harder breakdown. In fact, the entire range of such conditions can be experimentally realized by adding a resistance R_s in series with the stress voltage source [see Fig. 12(a)], and can be theoretically simulated by replacing AJ_{stress} in (3) with $(E - V)/R_s$. Constant current stress ($R_s = \infty$) and constant voltage stress ($R_s \approx 0$) represent two extremes of this configuration. Indeed, in Fig. 12(b) we find that, as predicted, the probability of soft breakdown increases with the increase in the series resistance. This increase in R_s gradually transforms a constant voltage source into a constant current source.

IV. THICKNESS SCALING

In the previous two sections, we have discussed how to translate the results of soft and hard breakdown as a function of area and stress voltage. Next we consider how the soft/hard breakdown fraction changes with oxide thickness, which could be useful for making predictions for future (yet-to-be-fabricated) gate oxides. To understand this scaling, consider Fig. 13 which shows that the applied voltage for thicker oxide (point B) must be larger than that of thinner oxide (point A) to produce the same prebreakdown stress current. Similarly, both Fig. 13 and our analysis in Section III show that thicker oxide requires slightly larger voltage (point D) than thinner oxide (point C) to produce the same postbreakdown percolation current. Notice that the difference in voltage to obtain equal percolation current, ΔV_{CD} is much smaller than that required to produce the same prebreakdown current ΔV_{AB} ; i.e., $V_C \sim V_D$, while $V_A < V_B$. Therefore, we expect that the postbreakdown voltages for constant current stress should be relatively thickness independent, which is confirmed by the experimental data in Fig. 14.

Fig. 13 can also be used to approximate the power dissipation for oxides with different thicknesses: since $P_{\text{thick}} [= I_B(V_B - V_D)] > P_{\text{thin}} [= I_A(V_A - V_C)]$ because $(V_B - V_A) > (V_D - V_C)$, thicker oxides will have harder breakdown than thinner oxides, which is again clearly validated by Fig. 14. More quantitatively, if we solve (3)–(7) (note the dependencies of the displacement current term [(4)], and percolation conductance term [(5) on thickness], the possible range of postbreakdown voltages

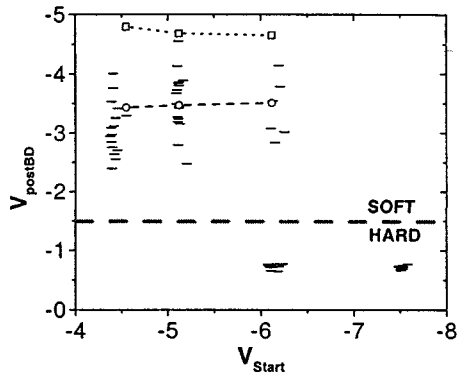


Fig. 14. Statistics of thickness dependence of oxide breakdown. To keep the prebreakdown current constant, the 3.5 nm oxides were stressed at ~ 4.5 V, 4.0 nm oxides at ~ 5.1 V, 5.0 nm oxides at ~ 6.1 V, and 6.5 nm oxides at ~ 7.5 V. The distribution of the stress voltage for each oxide thickness reflects a small distribution of oxide thicknesses around the mean value. Note that while the post-soft-breakdown voltage is almost thickness independent, the ratio of soft to hard breakdown is not, but rather shows strong thickness dependence. Simulation results based on (3)–(8) anticipate these trends (G_o^{\min} : dashed line, open circles; G_o^{\max} : dotted line, open squares).

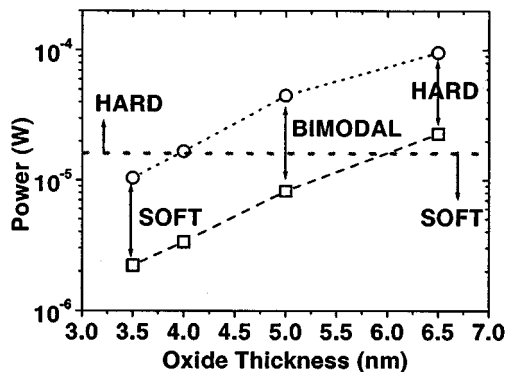


Fig. 15. Power dissipation (dotted line for G_o^{\max} , dashed line for G_o^{\min}) increases superlinearly with oxide thickness explaining the progressively harder breakdown with thickness. Note that the critical power density, $\sim 1.5 \mu\text{W}$, explains the transition of soft breakdown to hard breakdown as a function of oxide thickness.

predicted by the model (dashed and dotted lines, Fig. 14), corresponding to the statistical distribution of the percolation conductance, is consistent with the measurement. The conclusion that hard breakdown is more probable for thicker oxide, which has higher dissipated power (see Fig. 15), is also supported experimentally in Fig. 14. Also, the relative magnitudes of P_{perc} and $P_{\text{crit}} \sim 15 \mu\text{W}$ determines whether breakdown for a particular oxide thickness would be all soft, or all hard, or bimodal. However, note that for larger currents the theoretical predictions overestimate the experimental postbreakdown voltages. This is because, in solving (3)–(9), we assumed that G_o is time-independent, whereas in reality G_o increases moderately during the breakdown transient (Section III-A and Fig. 7 of [10]). This increase in G_o reduces the measured postbreakdown voltage.

When we stress the oxides at the same voltage so that thicker oxides (point B', Fig. 13) have lower prebreakdown current than thinner oxides (point A, Fig. 13). After breakdown, the final breakdown points are E and F which are relatively thickness-insensitive. The postbreakdown currents, measured

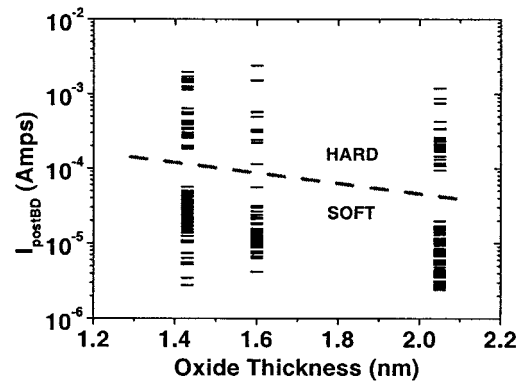


Fig. 16. For constant voltage stress for oxides with different thicknesses, both the postbreakdown currents as well as fraction of soft to hard breakdown events are almost independent of oxide thickness. The text explains why these trends are consistent with the theoretical analysis based on Fig. 13 and (3)–(8).

at 1.5 V and shown in Fig. 16, validate this expected thickness insensitivity. (e.g., $I_{\text{perc}} \sim 10^{-5}$ A). Moreover, we expect, again based on Fig. 13, the ratio of hard to soft breakdown to be almost thickness independent to the first order. This is because although $P_{\text{perc,thick}} = (I_E - I_A)V_A$ is slightly larger than $P_{\text{perc,thin}} = (I_F - I_{B'})V_A$, the $P_{\text{crit,thin}}$ is also slightly larger than $P_{\text{crit,thick}}$ (see discussion after (9) in [10]). Therefore, the ratios $\{P_{\text{perc,thick}}\}/P_{\text{crit,thick}} \sim \{P_{\text{perc,thin}}\}/P_{\text{crit,thin}}$ is relatively independent of thickness. Indeed, in Fig. 16, we see that the ratio of soft to hard breakdown remains relatively unchanged as a function of thickness, as predicted. Finally, if we compute the $P_{\text{crit}} = V_{\text{stress}}I_{\text{crit}}$ for these oxides, we find that $P_{\text{crit}} \approx 100 \mu\text{W}$. Compared to P_{crit} of 15–25 μW for 4-nm oxides, we do find that the critical power density increases with decreasing oxide thickness as anticipated in [10, Sect. II]. Note that since $V_{\text{crit}} = \sqrt{(P_{\text{crit}}/G_p)}$ and since G_p increases faster than P_{crit} for thinner oxides, the critical (transition) voltage would actually decrease with thickness.

V. POWER DISSIPATION VERSUS STORED ENERGY

We have explored the implications of changing the various terms of (3), by changing oxide thickness, stress current, capacitor area, etc. And we have seen that the predictions based on this model have consistently been satisfied. However, a specific aspect of our model that needs to be emphasized is the fundamental role of the dissipated power P_{perc} rather than the stored energy [8], [9], $(1/2)CV^2$ in determining the severity of oxide breakdown.

To test the proposition that P_{perc} is the relevant parameter, we add a large capacitor, C_{aux} , in parallel to the oxide under test (see Fig. 17). This addition increases the energy stored in the circuit by many orders of magnitude [see Fig. 18(a)]. Models that consider the total stored energy $(1/2)CV^2$ as the primary factor determining hard and soft breakdown would predict that adding a capacitor would result in significantly harder breakdown (statistically speaking). In contrast, our model predicts that since at constant voltage stress, the capacitors can not discharge their stored energy through the percolation path ($C(dv/dt) = 0$), the $\{P_{\text{perc}}\}$ must remain constant independent of C_{aux} (see Fig. 18(a), dotted and dashed line). Therefore, the addition of

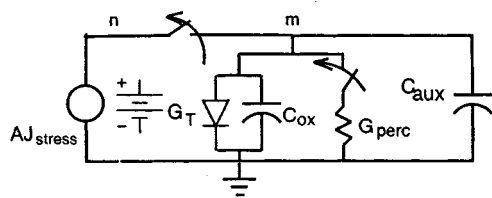
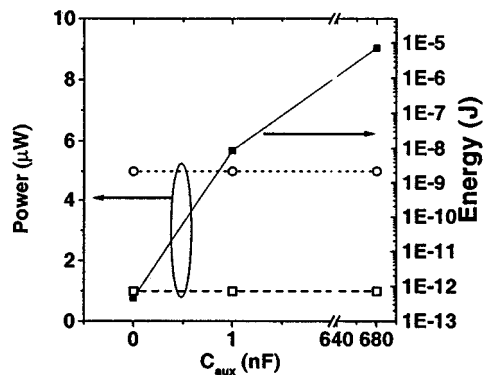
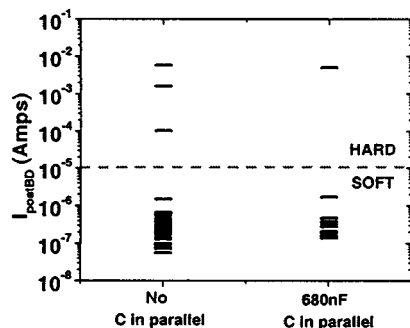


Fig. 17. Adding a large auxiliary capacitor in parallel to the oxide under test increases the stored energy (solid line) in the system without significantly increasing the power dissipation (dotted line for G_o^{\min} , dashed line for G_o^{\max}) through the oxide. This independent control of stored energy and power dissipation is needed to differentiate their relative importance.



(a)

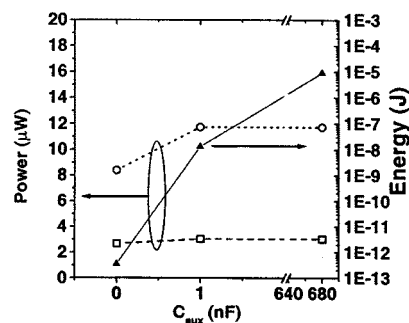


(b)

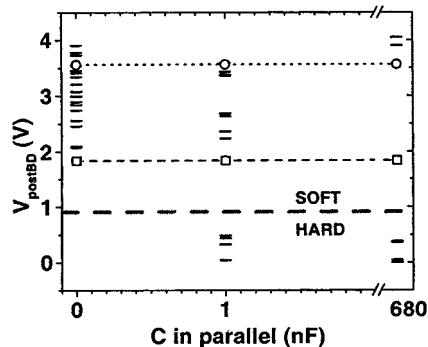
Fig. 18. (a) Adding a large parallel capacitor increases the stored energy (solid line), but does not increase the the power dissipation (dotted and dashed line) through the percolation path significantly. For constant voltage stress, power dissipation is independent of C_{aux} ; therefore, we do not expect any change in breakdown statistics due to this additional capacitor. (b) For constant voltage stress, the addition of the auxiliary capacitor plays no role in determining the ratio of soft to hard breakdown which is consistent with the theoretical considerations described in the text.

C_{aux} can play no role in determining breakdown statistics (see Section I). The experimental data shown in Fig. 18(b) supports our analysis: the fraction of hard to soft breakdown events remains unaltered even though the stored energy differs by six orders of magnitude between the two cases (see Fig. 18(a), filled squares).

Similarly, for constant current stress, adding a capacitor in parallel increases the stored energy significantly, [see Fig. 19(a), solid line, filled symbol], with only a modest increase in $\{P_{perc}\}$ [see Fig. 19(a), dotted line]. This is because C_{aux} increases both the stored energy, $(1/2)(C_{aux} + C_{ox})^2$ as well as the discharge time, $G_p(C_{aux} + C_{ox})$, keeping power dissipation, which is the ratio of the stored energy to the discharge time, the same



(a)



(b)

Fig. 19. (a) Similar to Fig. 18(a), adding a large parallel capacitor increases the stored energy (solid line). However, in contrast to Fig. 18(a), for constant current stress, the P_{perc} (dotted line for G_o^{\max} , dashed line for G_o^{\min}) increases with C_{aux} making harder breakdown more probable with larger auxiliary capacitance. (b) However, even with several orders of magnitude change in stored energy (solid line), the decrease in fraction of soft broken samples is small. The oxide thickness is 3.2 nm and the oxides are stressed at 2 A/cm², and the dashed and dotted lines (with symbols) are the theoretical predictors for V_{postBD} .

to zeroth order. However, since the discharge time is longer with a larger auxiliary capacitor, power dissipation is slightly higher at any given moment during the breakdown transient [see Fig. 19(b)]. Therefore, as we increase the value of the auxiliary capacitor, the proportion of hard breakdowns increases gradually. However, even after five orders of magnitude change in the stored energy ($C_{aux} = 1$ nF and $C_{ox} \sim 0.03$ pF), the ratio of soft to hard breakdown has not still changed significantly. Had the total stored energy been the determining factor, one would expected a stronger change in breakdown statistics with such a significant change in the stored energy.

VI. HARD BREAKDOWN AT 1 V FOR A 1.5 nm OXIDE

As an example application of the scaling principles discussed in Section I to V, we now compute the probability of hard breakdown for a 1.5-nm oxide operating at 1 V. Assume, conservatively, that $P_{crit} \sim 10 \mu W$, and the oxides are being stressed at constant voltage stress. Therefore, $I_{crit} = (P_{crit}/V_{stress}) = 10 \mu A$, which defines the critical current for hard breakdown at 1 V. To compute the probability of hard breakdown, we must now determine the number of 1.5 nm samples (as a fraction of the total sample size) whose postbreakdown current would exceed I_{crit} . To do so, one fits the pdf of the postbreakdown current distribution for a 1.5-nm oxide, taken at 1.5 V (see [10, Fig. 6] and Fig. 16), with an analytical expression. One may

then use the voltage scaling law, $I_{\text{perc}} = G_o V^\delta$ and the analytical pdf function to translate the distribution of percolation currents from 1.5 V to 1 V. Comparing the probability that the tail of the postbreakdown current distribution exceeds the critical current threshold of 10 μA , we find the possibility of hard breakdown to be negligible ($\ll 1 \times 10^{-15}$). This virtually guarantees that there will be no hard breakdown for 1.5-nm oxides at 1 V, especially since no area scaling will be involved (because severity of breakdown, for constant voltage stress, is essentially independent of oxide area (Fig. 4, Section II).

VII. CONCLUSION

A theory of soft and hard breakdown that can explain a wide range of experimental data has been proposed and verified. We have established, in Part I of this paper [10], a concrete connection between the percolation theory and the statistical distribution of the postbreakdown current (see [10, Sect. III]). We have also provided independent and direct experimental verifications of the existence and the dynamics of the percolation conductance. This connection between percolation theory and the postbreakdown $I-V$ data has, among other things, convincingly shown that the trap-diameter cannot exceed 1.5 nm.

This thorough understanding of the percolation conductance has in turn enabled us, also for the first time, to predict and to experimentally verify the hard and soft breakdown characteristics for oxides of different thickness, stress conditions, and capacitor area, all within a consistent theoretical framework of the breakdown transient. We not only explored the existing experimental data relevant to IC applications, but also conducted experiments inspired by the theoretical predictions, e.g., the consequences of adding a capacitor in parallel or a resistor in series. Based on the model, we conclude that soft breakdown will be the primary mode of device failure for small area transistors with ultrathin gate oxides and very low operating voltages, due to a significant decrease in power dissipation through the percolation path during the breakdown process. Also, by establishing the common statistical origin of soft and hard breakdown, we have demonstrated why one should consider the first breakdown, be it soft or hard, for the analysis of experiments involving voltage, area, and temperature acceleration. This model, therefore, can now be used to explore the role of soft-broken oxides in future MOSFET technologies, a topic we shall explore in a separate article in the future.

ACKNOWLEDGMENT

The authors would like to thank M. M. Brown, Y. Ma, D. Hwang, and A. Hamad for assistance with wafer preparation, A. Ghetti for tunneling simulation to determine oxide thickness, and R. Kent Smith for numerical software for matrix inversion used in the percolation calculations. The authors would also like to thank D. Frank, J. Suñé, T. Nigam, P. Peumans, G. Timp, and S. Hillenius for many stimulating discussions.

REFERENCES

- [1] B. Weir *et al.*, "Ultrathin gate dielectrics: They break down, but do they fail?," in *IEDM Tech. Dig.*, 1997, pp. 73–76.

- [2] E. Wu, K. Nowak, J. Aitken, W. Abadeer, L. K. Han, and S. Lo, "Structural dependence of dielectric breakdown in ultrathin gate oxides and its relationship to soft broken modes and device failure," in *IEDM Tech. Dig.*, 1998, pp. 187–190.
- [3] T. Pompl, H. Wurzer, M. Kerber, W. Wilkins, and I. Eisele, "Influence of soft breakdown on NMOSFET device characteristics," in *Proc. 37th IRPS Conf.*, 1999, pp. 82–87.
- [4] F. Crupi, R. Degraeve, G. Groeseneken, T. Nigam, and H. Maes, "On the properties of the gate and substrate current after soft breakdown in ultrathin oxides layers," *IEEE Trans. Electron Devices*, vol. 45, pp. 2329–2334, Dec. 1998.
- [5] K. Okada, "The gate oxide lifetime limited by 'B-Mode' stressed induced leakage current and the scaling limit of silicon dioxide in the direct tunnelling region," *Semicond. Sci. Technol.*, vol. 15, pp. 478–484, 2000.
- [6] S. Bruyère, E. Vincent, and G. Ghibaudo, "Quasi-breakdown in ultrathin SiO_2 films: Occurrence characterization and reliability assessment method," in *Proc. 38th IRPS Conf.*, 2000, pp. 48–54.
- [7] M. Alam, B. Weir, J. Bude, P. Silverman, and D. Monroe, "Explanation of soft and hard breakdown and its consequences for area scaling," in *IEDM Tech. Dig.*, 1999, pp. 449–452.
- [8] J. Jackson, "Electrical breakdowns and breakdown mechanisms in ultrathin silicon dioxides," *Microelectron. Reliab.*, vol. 39, pp. 171–179, 1999.
- [9] J. C. Jackson, T. Robinson, O. Oralkan, D. J. Dumin, and G. A. Brown, "Differentiation between electric breakdowns dielectric breakdown in thin silicon oxides," *J. Electrochem. Soc.*, vol. 145, no. 3, pp. 1033–1038, 1998.
- [10] M. A. Alam, B. E. Weir, and P. J. Silverman, "A study of soft and hard breakdown—Part I: Analysis of statistical percolation conductance," *IEEE Trans. Electron Devices*, vol. 49, pp. 232–238, Feb. 2002.



Muhammad Ashraf Alam (M'97–SM'01) was born in Dhaka, Bangladesh, in 1964. He received the B.S.E.E. degree from Bangladesh University of Engineering and Technology in 1988, the M.S. degree from Clarkson College of Technology, Potsdam, NY, in 1991, and the Ph.D. degree from Purdue University, West Lafayette, IN, in 1994, all in electrical engineering.

From 1995 to 2000, he was with Bell Laboratories, Lucent Technologies, as Member of Technical Staff in the Silicon ULSI Research Department. Currently,

he is a Distinguished Member of Technical Staff of Agere Systems, Murray Hill, NJ, a spin-off of Lucent Technologies which specializes in the manufacture of electronic and optoelectronic devices. His research interest involves the physics of carrier transport in semiconductor devices, and he has worked on theoretical aspects of transport models, quasi-ballistic transport in bipolar transistors, MOCVD crystal growth, laser dynamics, and most recently, on the theory of oxide reliability.

Bonnie E. Weir (M'95) was born in Osaka, Japan, in 1965. She received the B.A. degree (with honors) in physics from Swarthmore College, Swarthmore, PA, in 1988, and the Ph.D. degree in physics from Stevens Institute of Technology, Hoboken, NJ, in 1994.

From 1988 to 2001, she was Member of Technical Staff at Bell Laboratories, working for AT&T and then Lucent Technologies. She is currently with Agere Systems, Murray Hill, NJ. Her former research areas include Rutherford backscattering and boron δ -doping. She is currently active in experimental research on ultrathin oxide reliability. She holds a patent on dielectric breakdown detection and has authored or coauthored more than 50 technical papers.

Paul J. Silverman was born in Philadelphia, PA, in 1948. He received the B.S. degree in physics from Drexel University, Philadelphia, and the M.S. degree in physics from Purdue University, West Lafayette, IN.

He joined Bell Laboratories in 1969, where he worked on loudspeaker design, Rutherford backscattering spectrometry, scanning tunneling microscopy, and molecular beam epitaxy. He is now working on electrical device characterization and dielectric reliability testing at Agere Systems (formerly Lucent Technologies' Microelectronics division), Murray Hill, NJ.